Earth and Planetary Science Letters 461 (2017) 73–84

Contents lists available at ScienceDirect

Earth and Planetary Science Letters

www.elsevier.com/locate/epsl

The arc arises: The links between volcanic output, arc evolution and melt composition

Philipp A. Brandl [a,b,*], Morihisa Hamada [c,d], Richard J. Arculus [b], Kyle Johnson [e], Kathleen M. Marsaglia [e], Ivan P. Savov [f], Osamu Ishizuka [d,g], He Li [h]

[a] GEOMAR Helmholtz Centre for Ocean Research Kiel, Wischhofstr. 1-3, 24148 Kiel, Germany
[b] Research School of Earth Sciences, The Australian National University, 142 Mills Road, Acton ACT 2601, Australia
[c] Department of Solid Earth Geochemistry, Japan Agency for Marine–Earth Science and Technology, 2-15 Natsushima-cho, Yokosuka 237-0061, Japan
[d] Research and Development Center for Ocean Drilling Science, Japan Agency for Marine–Earth Science and Technology, 2-15 Natsushima-cho, Yokosuka 237-0061, Japan
[e] Department of Geological Sciences, California State University Northridge, 18111 Nordhoff Street, Northridge, CA 91330-8266, USA
[f] School of Earth and Environment, The University of Leeds, Institute of Geophysics and Tectonics, Leeds LS2 9JT, United Kingdom
[g] Geological Survey of Japan/AIST, Central 7 1-1-1 Higashi, Tsukuba, Ibaraki 305-8567, Japan
[h] Guangzhou Institute of Geochemistry, Chinese Academy of Sciences, 511 Kehua Street, Wushan Guangzhou 510640, China

ARTICLE INFO

Article history:
Received 4 November 2016
Received in revised form 18 December 2016
Accepted 19 December 2016
Available online xxxx
Editor: T.A. Mather

Keywords:
Izu–Bonin
U1438
mantle wedge
subduction
island arc
melt inclusion

ABSTRACT

Subduction initiation is a key process for global plate tectonics. Individual lithologies developed during subduction initiation and arc inception have been identified in the trench wall of the Izu–Bonin–Mariana (IBM) island arc but a continuous record of this process has not previously been described. Here, we present results from International Ocean Discovery Program Expedition 351 that drilled a single site west of the Kyushu–Palau Ridge (KPR), a chain of extinct stratovolcanoes that represents the proto-IBM island arc, active for ~25 Ma following subduction initiation. Site U1438 recovered 150 m of oceanic igneous basement and ~1450 m of overlying sediments. The lower 1300 m of these sediments comprise volcaniclastic gravity-flow deposits shed from the evolving KPR arc front. We separated fresh magmatic minerals from Site U1438 sediments, and analyzed 304 glass (formerly melt) inclusions, hosted by clinopyroxene and plagioclase.

Compositions of glass inclusions preserve a temporal magmatic record of the juvenile island arc, complementary to the predominant mid-Miocene to recent activity determined from tephra layers recovered by drilling in the IBM forearc. The glass inclusions record the progressive transition of melt compositions dominated by an early 'calc-alkalic', high-Mg andesitic stage to a younger tholeiitic stage over a time period of 11 Ma. High-precision trace element analytical data record a simultaneously increasing influence of a deep subduction component (e.g., increase in Th vs. Nb, light rare earth element enrichment) and a more fertile mantle source (reflected in increased high field strength element abundances). This compositional change is accompanied by increased deposition rates of volcaniclastic sediments reflecting magmatic output and maturity of the arc. We conclude the 'calc-alkalic' stage of arc evolution may endure as long as mantle wedge sources are not mostly advected away from the zones of arc magma generation, or the rate of wedge replenishment by corner flow does not overwhelm the rate of magma extraction.

1. Introduction

Subduction initiation and accompanying onset of arc magmatism are critical processes in global plate tectonics. However, the precise temporal, spatial, and compositional evolution of the early stages of island arc magmatism are poorly understood even though they play a major role in the generation of new continental crust (Davidson and Arculus, 2005). The first magmatic products related to subduction initiation in the Izu–Bonin–Mariana (IBM) subduction system (Fig. 1) are 52–48 Ma basalts exposed on the arc-ward trench wall and have accordingly been termed forearc basalts (FAB) (e.g., Ishizuka et al., 2011a; Reagan et al., 2010). A FAB-like igneous basement of similar age was penetrated in a rearare position at International Ocean Discovery Program (IODP) Site U1438; this

* Corresponding author at: GEOMAR Helmholtz Centre for Ocean Research Kiel, Wischhofstr. 1-3, 24148 Kiel, Germany.
E-mail address: pbrandl@geomar.de (P.A. Brandl).

http://dx.doi.org/10.1016/j.epsl.2016.12.027

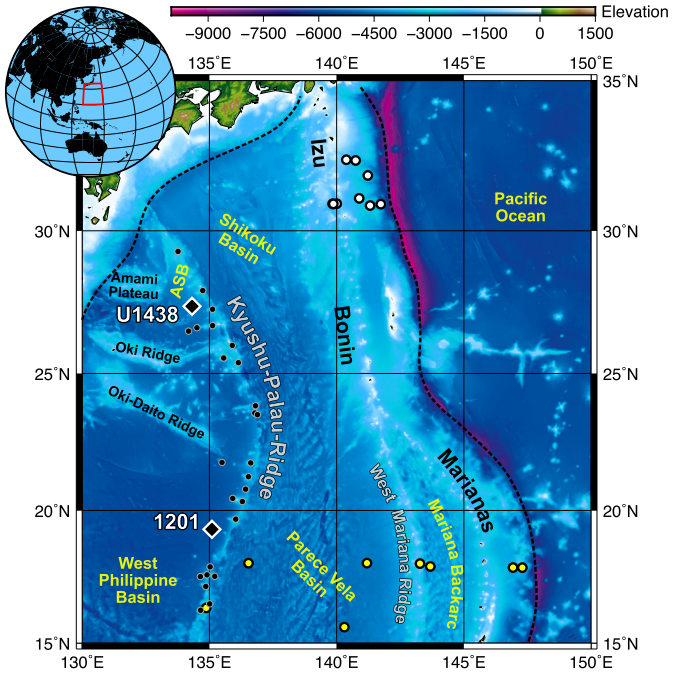

Fig. 1. Bathymetric map with key geological features of the northern Izu–Bonin–Mariana subduction system and locations of Sites U1438 (IODP Expedition 351) and 1201 (ODP Expedition 195). ASB: Amami Sankaku Basin. Grey dots correspond to drilled/dredged samples of the KPR with age data (Ishizuka et al., 2011b), white dots represent Izu–Bonin tephra samples recovered from ODP Sites 782, 784, 786–788, 790–793 and yellow dots represent Mariana arc tephra recovered from DSDP Sites 53 and 54 and ODP Sites 448, 449, 451, 453, 458, 459. (For interpretation of the references to color in this figure legend, the reader is referred to the web version of this article.)

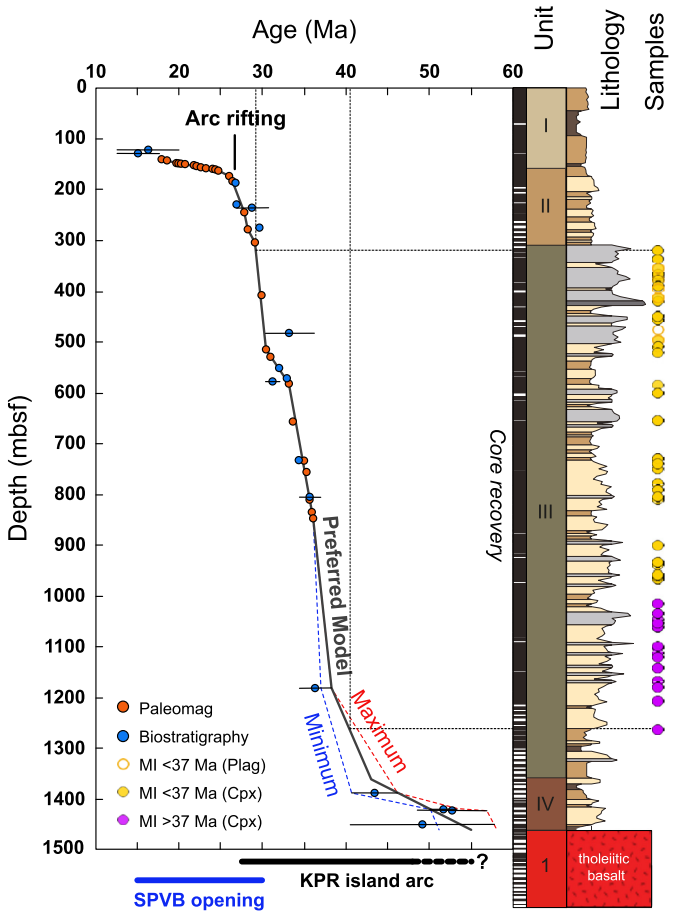

Fig. 2. Overview of the drilled sequence at Site U1438, sampling intervals and age constraints from paleomagnetic and paleontological onboard studies (Arculus et al., 2015b) plotted versus depth (in meters below seafloor). Our preferred age versus depth model is shown by a black line and the limits of uncertainty in the lower part of the sequence are illustrated by a red (maximum) and blue (minimum) dashed line. Note that in the core recovery column, white intervals represent gaps in core recovery, indicating that the Unit III interval sampled in this study is remarkably complete. Note that the paleomagnetic ages represent the depth of each geomagnetic polarity timescale chron and thus do not include uncertainties. (For interpretation of the references to color in this figure legend, the reader is referred to the web version of this article.)

magma type was clearly extensively distributed both along- and across-strike of the proto-IBM arc (Arculus et al., 2015a, 2016). The bathymetry, crustal structure, and pre-IBM sediments in basins between the Mesozoic–Lower Cenozoic arc ridges (Amami Plateau, Daito and Oki-Daito) west of Site U1438 show no sign of compressional uplift and sediment shedding, consistent with subsidence and extensional rifting accompanying a spontaneous mode of subduction inception for the IBM system (Leng and Gurnis, 2015; Arculus et al., 2016).

The timing of subduction initiation has been dated at ~52 Ma (e.g., Ishizuka et al., 2006, 2011a). Subsequent formation of new oceanic igneous crust (submarine lava flows, sheeted dyke complex and plutonic gabbros) with a FAB-like geochemical signature lasted for 2–4 Ma. In the arc-ward trench wall of the Izu–Bonin (Ishizuka et al., 2011a) and Mariana trenches (Reagan et al., 2010), FABs are overlain first by low-silica boninites and high-magnesia andesites followed by high-silica boninites (e.g., Pearce et al., 1992; Kanayama et al., 2014; Reagan et al., 2015). This type of magmatism lasted for about 4 Ma and then from 44 Ma onwards (~8 Ma after subduction initiation), volcaniclastic sediments indicative of arc maturation and volcanic edifice (i.e., stratovolcano) buildup and erosion are preserved in the IBM forearc.

The important phenomena we address in this paper relate to the post-subduction initiation evolution of the volcanic arc system, the subarc mantle and slab sources. We compare our results from IODP Site U1438 with comparable rock suites recovered from other IBM sites via dredging or drilling. Our aim is to investigate magmatic evolution and provincialism during the early phase of intra-oceanic island arc volcanism in the western Pacific because a corresponding detailed record of volcanic arc products has been recovered neither from the Kyushu–Palau Ridge (KPR) nor the active IBM island arc. In fact, geologic records of the juvenile arc are sparse and previously restricted to settings in the present forearc (e.g., Ishizuka et al., 2006; Reagan et al., 2008). Thus, Site U1438 (Fig. 1) in the Amami Sankaku Basin represents probably the best and most complete record of island arc evolution beginning with subduction initiation in the Early Eocene to arc rifting and backarc opening in the Late Oligocene and Early Miocene.

Furthermore, the volcaniclastic record at Site U1438 provides a more complete and also 'averaged' record of the magmatic evolution of island arcs than individual lava flows (Gill et al., 1994). Widely disseminated ash preserves the best 'averaged' record of island arc evolution but is highly biased to explosive volcanism and thus the highly evolved end of melt compositions and lack spatial information. Turbidites, in contrast, can be linked to some degree via seismic stratigraphy (e.g., thickening of depositional units towards volcanic edifices) and their rapid transport and burial minimizes chemical alteration prior to deposition (Gill et al., 1994). Our study focuses on glass inclusions hosted in fresh clinopyroxene and minor plagioclase crystals that span a depositional age from 29 to 40 Ma (Fig. 2). This 11 Ma long record of early arc magmatism sourced from the proto-IBM (KPR) is a key to further our understanding of island arc evolution and mass transfer in subduction zones.

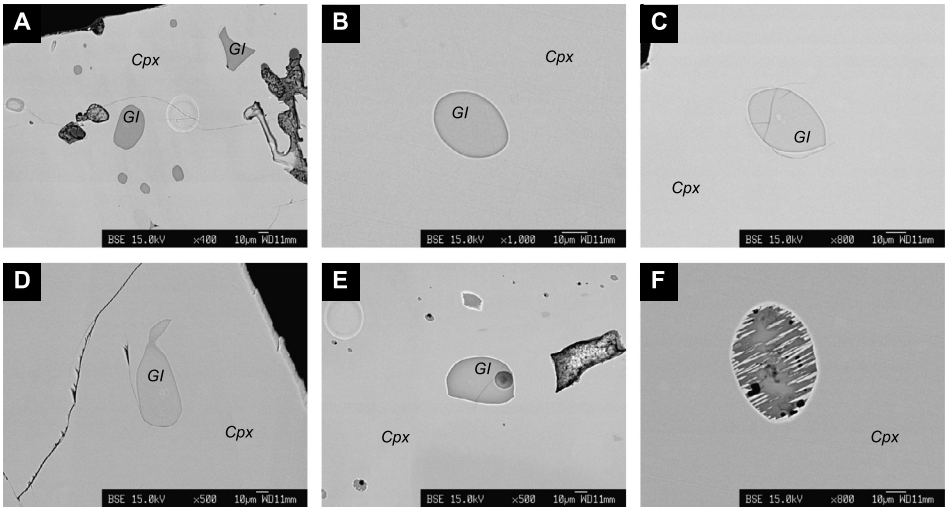

Fig. 3. Representative BSE images of glass inclusions hosted in clinopyroxene. A) Several glass inclusions with variable shapes in a clinopyroxene (U1438E-13R-CC, 31–34 cm). B) Pristine glass inclusion (U1438E-13R-2W, 82–85 cm). C) Pristine glass inclusion with cooling cracks (U1438E-34R-4W, 93–95 cm). D) Pristine glass inclusion with a highly irregular shape (U1438E-27R-5W, 55–58 cm). E) Glass inclusion with a large shrinkage bubble and rims possibly altered by post-entrapment processes (U1438E-34R-4W, 93–95 cm). F) Fully crystallized and altered (former glass) inclusion (U1438E-13R-2W, 82–85 cm). Note that LA-ICPMS spots in A) and E) are from recent trace element analyses and are for targeting purpose only (single shot).

2. Material and methods

2.1. IODP Expedition 351 Izu–Bonin–Mariana arc origins

IODP Expedition 351 aimed to recover material related to the inception of the Izu–Bonin–Mariana (IBM) island arc in the Early Eocene by drilling a single site into the sediments and the basement of the Amami Sankaku Basin (Fig. 1). The expedition successfully drilled >1,450 m of hemipelagic (Unit I) and volcaniclastic (Units II–IV) sediments overlying 150 m of oceanic igneous basement (Unit 1; Fig. 2). The igneous basement is interpreted as having formed during subduction initiation (Arculus et al., 2015a, 2015b), and the overlying sedimentary units thicken towards and were likely sourced from the KPR (remnants of the proto-IBM arc) which bounds the Amami Sankaku Basin to the east (Fig. 1). The igneous basement provides direct information on the process and dynamics of subduction initiation; it is overlain by a ∼100 m thick unit (Unit IV) of deep-sea mudstones intercalated with volcaniclastic gravity-flow deposits (Arculus et al., 2015b) and volumetrically minor intrusive rocks. This sequence we propose reflects the onset of island arc volcanism driven by slow edifice growth and via gravity flow-driven deposition of pyroclastic-rich materials. Preliminary age constraints on Unit IV are insufficient to precisely date the earliest volcaniclastic deposits but probably overlaps to some extent the episode of boninitic volcanism preserved in the IBM forearc (e.g., Ishizuka et al., 2011a; Reagan et al., 2010).

Overlying Unit IV is a 1,184 m thick sequence (Units II+III; Fig. 2) of mainly volcaniclastic gravity-flow deposits (Arculus et al., 2015b) that accumulated during the active phase of volcanism along the KPR. Volcanism at the KPR prevailed for ∼18 Ma (Ishizuka et al., 2011b) following subduction initiation and ceased when intra-arc rifting split the KPR and spreading began in the Shikoku and Parece Vela Basin (SPVB) at ∼25 Ma (Ishizuka et al., 2011b; Fig. 2). The timeframe of active magmatism at the KPR (Ishizuka et al., 2011b) corresponds very well with observations from IODP Expedition 351 in terms of paleomagnetic and biostratigraphic age determinations and type of recovered sediments (Arculus et al., 2015a, 2015b; Fig. 2). In total, we sampled 56 coarse-grained (minimum grain size: medium sand) intervals in Unit III to construct a complete record of volcanism along the KPR (29.29–40.25 Ma; Fig. 2).

Shipboard analysis of the Site U1438 cores completed a comprehensive mineralogical, lithological and structural description (Arculus et al., 2015b). Post-expedition research has defined sedimentary facies and includes interpretations of sedimentary depositional processes (Johnson, 2016). These results are summarized in supplementary Table S1. Biostratigraphic and paleomagnetic datums are abundant throughout Units I–II and the upper half of Unit III, allowing us to determine the precise ages of sediment deposition ∼850 mbsf but requiring some extrapolation from 850 mbsf to the basement (Fig. 2; supplementary information).

2.2. Glass inclusion analyses

Volcaniclastic sediments were disintegrated using SELFRAG® high-voltage pulse power fragmentation at JAMSTEC. The majority of minerals are clinopyroxene (cpx) with minor plagioclase (plag), quartz, amphibole, and pigeonite. No olivine is preserved. Visual assessment of the mineral separates and also shipboard XRD analyses (Arculus et al., 2015b) indicate an increasing proportion of quartz with stratigraphic younging (i.e. <1050 mbsf). Individual crystals were mounted in epoxy and especially notable are the abundant glass inclusions preserved in clinopyroxene (Fig. 3A) that can be exposed at surface by hand polishing. Most of these glass inclusions are round in shape and pristine (Fig. 3B, C). Inclusions with irregular or angular shape (Fig. 3D) or those exhibiting shrinkage bubbles (Fig. 3E) were carefully examined and rejected if post-entrapment alteration (e.g., crystallization of the trapped melt; Fig. 3F) was observed (see also Fig. S1).

Major element compositions of glass inclusions and mineral hosts were obtained using well established electron microprobe techniques at the GeoZentrum Nordbayern (FAU Erlangen-Nürnberg), the Research School of Earth Sciences (RSES, ANU Canberra) and JAMSTEC. At the GeoZentrum Nordbayern, major element analyses were performed using a JEOL JXA-8200 Superprobe following standard techniques (15 kV acceleration voltage, 15 nA beam current and 10 µm beam diameter for glasses, 3 µm for silicates). Sulfur contents of the corresponding glass inclusions have been determined at RSES using a peak scan method to account for possible shifts in the redox-dependent Kα peak position. At both facilities, the Smithsonian Institute standard glass VG-2 was continuously monitored. At JAMSTEC, major element analyses were performed under the same conditions using a JEOL

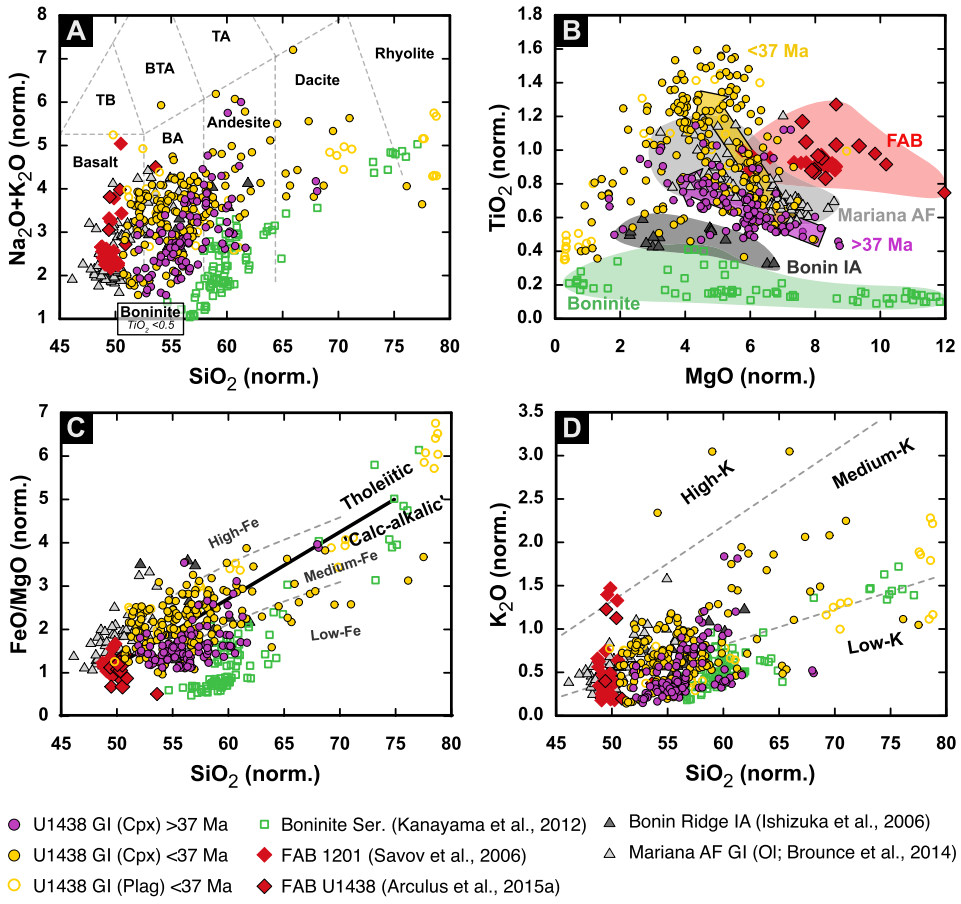

Fig. 4. A) Total alkalis (Na_2O+K_2O) versus SiO_2 diagram after Le Bas et al. (1986). B) TiO_2 versus MgO. Note the great difference in the shape of the differentiation trends between the distinct rock series and the two groups <37 and >37 Ma in particular. C) FeO^T/MgO versus SiO_2. Low-Fe, medium-Fe and high-Fe association after Arculus (2003) and tholeiitic-'calc-alkalic' divide after Miyashiro (1974). D) K_2O versus SiO_2 diagram after Le Maitre et al. (1998). All data volatile-free and normalized to a total of 100 wt.%. Data sources: Boninite Series from the Bonin Ridge: Kanayama et al. (2012); FAB 1201: ODP Site 1201: Savov et al. (2006) (altered samples excluded); FAB U1438: IODP Site U1438: Arculus et al. (2015a); Bonin Ridge IA: high-Mg/island arc tholeiitic/'calc-alkalic' andesites: Ishizuka et al. (2006); Mariana AF GI (olivine-hosted glass inclusions from the modern Mariana Arc Front): Brounce et al. (2014).

JXF-8500F electron microprobe. Analytical results were monitored *in situ* by comparing with the analytical results of MPI-DING reference glasses (Jochum et al., 2000).

Trace element analyses were performed at RSES using the newly installed Coherent CompexPro 110 laser ablation system connected online to an Agilent 7700 quadrupole ICPMS. A 28 µm spot size was used in all analyses (40 s ablation time) with Ca as an internal standard, NIST glass 610 for drift correction and standard glasses NIST-612 and BCR-2G as external reference materials. Results from geochemical analyses of all samples and reference materials are presented in supplementary Table S2. See also the supplementary information for further details (e.g., glass inclusion EMP profiles, Fig. S2).

3. Results

No glass inclusions with visible reaction rims or a microcrystalline matrix were analyzed, resulting in 326 glass analyses from inclusions varying in size from 25 to 153 µm. The majority (295) are hosted in clinopyroxene (cpx) with mainly augitic and minor diopsidic mineral compositions (Table S2). These host crystals range in Mg# from 91.6 to 68.4 (Table S2; Fig. S3) and in TiO_2 from 0 to 0.8 wt.% (Fig. S4). Another 31 glass inclusions are hosted in plagioclase of variable anorthite content (93.5 to 42.6) but these feldspars are restricted to the interval between 350 and 500 mbsf.

Glass inclusions that yielded major element totals of 90 wt.% or less have been rejected from our dataset. Furthermore, the partitioning of the Fe–Mg exchange between glass inclusion and cpx host crystal (0.27 ± 0.03; Putirka, 2008; Fig. S3) has been used as a criterion to exclude a few erratic inclusions with unusual low Mg#s with respect to their cpx host. Based on these criteria, 22 out of the 326 glass inclusions analyzed were rejected from the final dataset. Even though, post-entrapment alteration cannot be completely ruled out, compositional similarity of plagioclase- and cpx-hosted glass inclusions over the respective interval is another independent measure of the post-entrapment, compositional inertness of the inclusions and robustness of our analytical data.

Analyses of the remaining 304 glass inclusions show a wide range of magmatic differentiation from basalt to rhyolite (Fig. 4A). Glass inclusions are well correlated in TiO_2 with their respective cpx hosts (Fig. S4). These inclusions show a broad trend towards more differentiated compositions (i.e., lower Mg#) with stratigraphic younging (Fig. S5) and trapped melts with MgO contents as high as 8.75 wt.% (Fig. S6). Furthermore, the wide range of major oxide compositions when compared at similar indices of magmatic differentiation is remarkable: TiO_2, for example, varies from <0.4 to 1.6 wt.% between 5.0 to 6.0 wt.% MgO (Fig. 4B). Based on their major element composition, two glass inclusions from core U1438-27R-5W (~1096 mbsf) fall just inside the field of boninites as defined by Le Bas (2000; Fig. 4A). These inclusions have FeO^T/MgO of <1.2 and MgO >8.0 wt.% and thus represent the most primitive end-member of the low-Fe (Arculus, 2003) or 'calc-alkalic' trend amongst the glass inclusion population (Fig. 4C). Most of the glass inclusions sampled from the lower part of Unit III

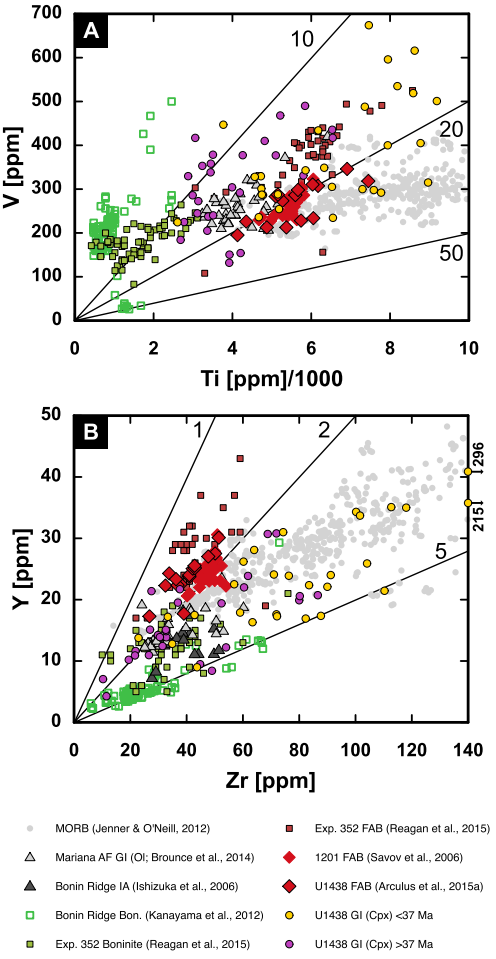

Fig. 5. A) V vs. Ti, B) Y vs. Zr as used by Arculus et al. (2015a) to discriminate between the different rock suites. Data sources: Exp. 352 Boninites and FAB: Reagan et al. (2015); MORB: Jenner and O'Neill (2012), filtered for MOR origin; Other data sources as in Fig. 3.

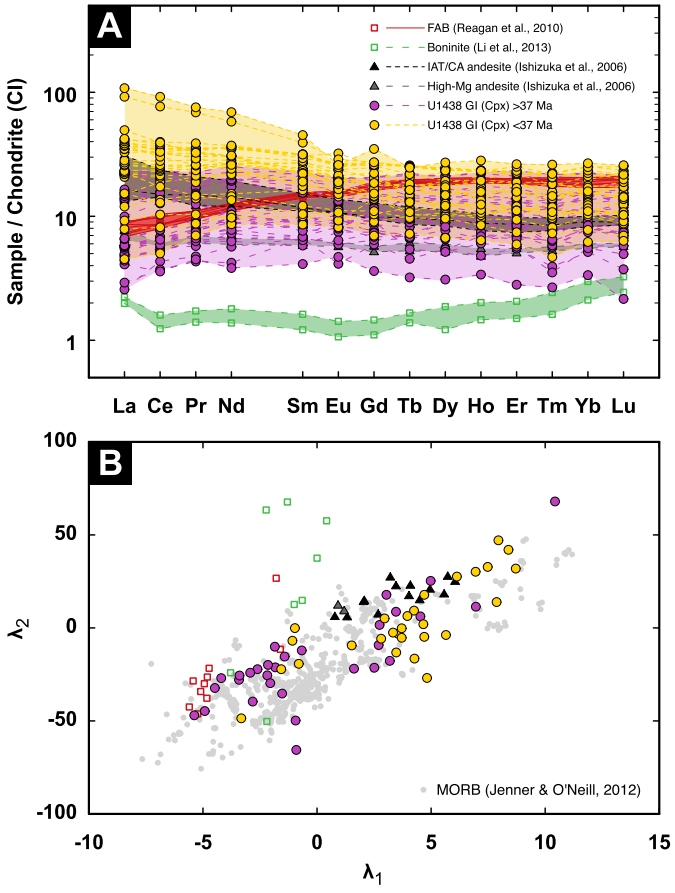

Fig. 6. A) CI-normalized rare earth element pattern for clinopyroxene-hosted glass inclusions of Site U1438. Chondrite normalizing values of McDonough and Sun (1995). B) REE pattern shape coefficients λ_2 vs. λ_1 (O'Neill, 2016). Note the overall diversity of U1438 data relative to global MORB (data as in Fig. 4). High-Mg andesite and island arc tholeiitic/'calc-alkalic' andesites of Ishizuka et al. (2006) and some representative patterns for FAB (Reagan et al., 2010) and Boninite (Li et al., 2013) are shown for comparison.

(>1000 mbsf or older than 37 Ma) have lower total alkali contents (K_2O+Na_2O; i.e., low-K association) when compared to inclusions shallower in the sequence (Figs. 4A, D) and belong to the low- and medium-Fe trends (Fig. 4C). In contrast, inclusions from samples collected from the upper Unit III (<1000 mbsf and younger than 37 Ma) tend to have lower SiO_2 and higher total alkali contents (Fig. 4A), belong to the medium- and high-Fe trends (i.e., tholeiite series; Fig. 4C) and are part of the medium-K association (Fig. 4D). 'Classic' Harker plots can be found in Fig. S6.

Although there is compositional overlap, trace element analyses of 58 representative glass inclusions reveal some persistent differences between the <37 and >37 Ma groups. Plots of V vs. Ti and Y vs. Zr are used to discriminate between boninites, forearc basalts and mid-ocean ridge basalts (Fig. 5; e.g., Arculus et al., 2015a; Reagan et al., 2015; Shervais, 1982). Here, most of the group >37 Ma shows a similar trajectory to boninites (V/Ti: ~10, Fig. 5A; Y/Zr: ~2, Fig. 5B) but offset to slightly higher incompatible trace element concentrations (Fig. 5). The group <37 Ma shows a wide range of compositions and is more similar to the MORB field in Y vs. Zr (Fig. 5B). Furthermore, chondrite-normalized rare-earth element (REE) patterns (Fig. 6A) are flat in the group >37 Ma. Patterns of the group <37 Ma are generally offset to higher concentrations but also skewed as a result of light REE enrichment relative to the heavy REE (Fig. 6A). These differences are also obvious using the REE pattern shape coefficients of O'Neill (2016; Fig. 6B). The group >37 Ma preferably plots towards the bottom left-hand corner of the diagram (strongly depleted LREE; concave downward) and the group <37 Ma towards the upper right-hand corner (enriched in LREE, concave upwards; Fig. 6B).

Significant differences between these two groups are also evident from trace elements that, according to Pearce et al. (2005), are controlled by shallow subduction (i.e. fluids, e.g. Ba), deep subduction (i.e. sediments, e.g. Th) or asthenosphere fertility (e.g., Nb). The behavior of these elements (and relative to Yb as a conservative heavy REE) is presented in Fig. 7: most of the samples from the group >37 Ma have steeper trajectories in Ba vs. Nb (Fig. 7A) compared to the group <37 Ma but similar Th vs. Nb (Fig. 7B).

Results from sedimentary facies analyses of volcaniclastic material at Site U1438 (e.g., Johnson, 2016) are summarized in supplementary Table S1. With the exception of some primary tuff layers, the sedimentary succession comprising Units II and III at Site U1438 consists of silty to sandy to gravel-bearing gravity-flow deposits, ranging from turbidites to debrites. These flows were likely sourced near volcanic edifices in the KPR, and traveled 10s of km beyond proximal volcanic apron facies as described in the literature (e.g., Houghton and Landis, 1989; Allen et al., 2007). Deposition at Site U1438 formed a series of at least 12 stacked lobe systems during 4 individual episodes, each lasting 1.6–2.0 Ma and separated by phases of relative quiescence (Johnson, 2016). Sedimentation rates were calculated for each individual facies-based division (Table S1; Johnson, 2016) and show a major spike in sediment accumulation younger than 37.75 Ma (or <1202.7 mbsf). De-

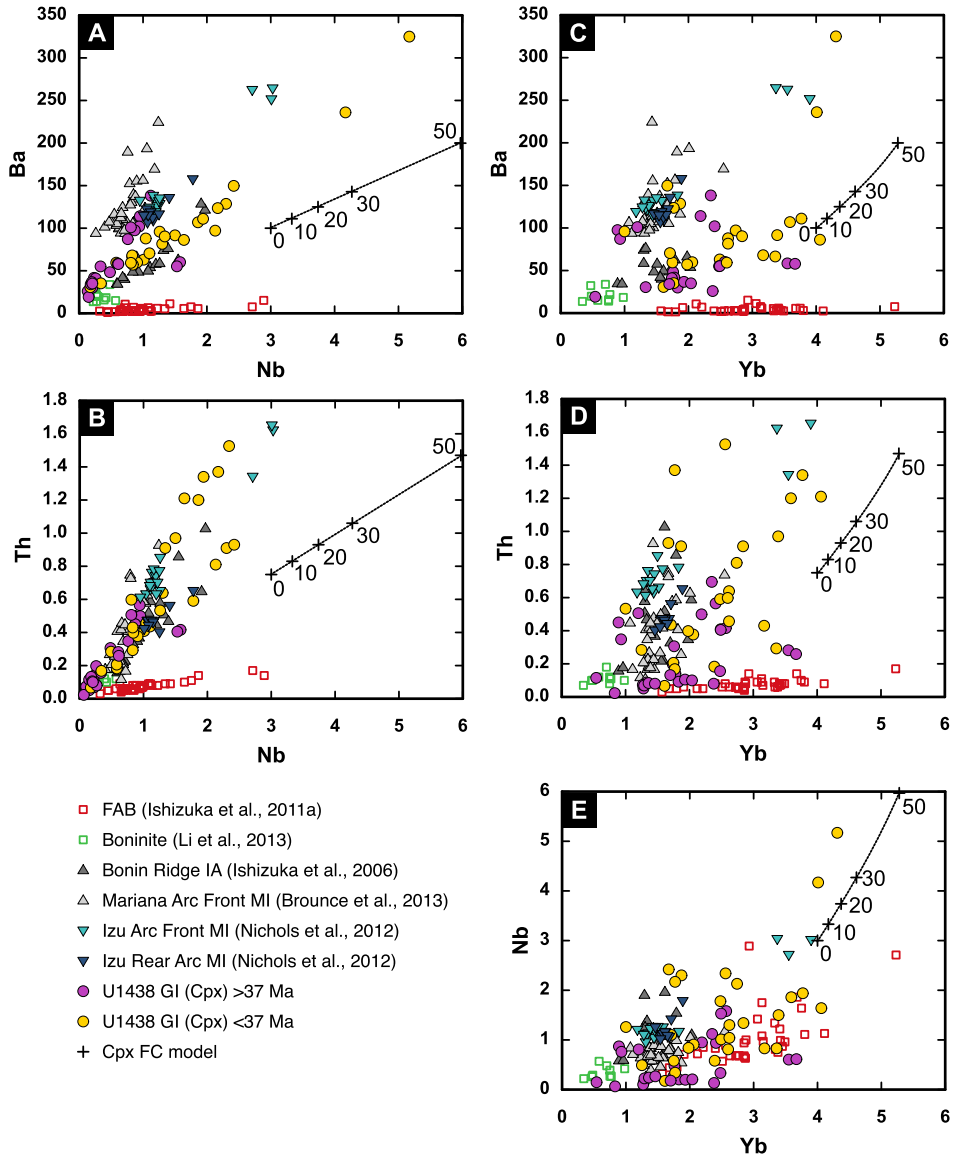

Fig. 7. A) Ba and B) Th vs. Nb. C) Ba, D) Th and E) Nb vs. Yb. Data sources: FAB: Ishizuka et al. (2011a); Boninite (Li et al., 2013); Bonin Ridge: Ishizuka et al. (2006); Olivine-hosted glass inclusions from the Mariana arc front: Brounce et al. (2014); Olivine-hosted glass inclusions from the Izu arc front and reararc: Nichols et al. (2012). Details of the clinopyroxene fractional crystallization model can be found in the supplementary information. Numbers indicate Vol. % of crystallization with "0" marking the starting composition chosen for illustration purpose of the FC trend only.

position rates remained constantly high (generally $>>50$ m Ma^{-1}) until 28 Ma (237.9 mbsf), before the input of volcaniclastic gravity-flows ceased and sedimentation became hemipelagic with accumulation rates of <10 m Ma^{-1} (Table S1).

4. Discussion

4.1. Age constraints and deposition history

Precise constraints on relative and absolute ages and the deposition mechanisms of the volcaniclastic sediments are crucial for the interpretation of the chemical composition and the evolution of island arc magmatism through time. Depositional ages have been constrained through paleomagnetic and micropaleontological data (Arculus et al., 2015b) and correlate well with published ^{40}Ar/^{39}Ar ages for the KPR. Ishizuka et al. (2011b) dated the active phase of the KPR (over its 2600 km strike length) to the time between 48 and 25 Ma. However, most exposed volcanism is limited to the final phase of 25–28 Ma that is recorded by the sharp decrease in deposition rate at Site U1438 (Fig. 2). The oldest sedimentary ages at Site U1438 (Fig. 2) are likely to be older than the 48 Ma reported for the onset of volcanism at the KPR (Ishizuka et al., 2011b).

However, a careful consideration of transport mechanisms and deposition environment is required for the interpretation of the geologic record of Site U1438. First of all, stratigraphic information at Site U1438 from 900 mbsf depth and further down is limited and requires some extrapolation (Fig. 2, supplementary information). In reality, if gravity flow events have a consistent frequency, then intervals with thick events should have higher accumulation rates (e.g., Cores 7R-13R and 21R-29R in Hole U1438E, whereas intervals of thinner units (e.g., Cores 4R-6R and 45R-54R in Hole U1438E) should have lower accumulation rates. Ages would be slightly overestimated in the former and underestimated in the latter. Even though the absolute rates of deposition are highly dependent on the precise slope of the age-depth curve, the general pattern is consistent through all models and is thus considered to be robust (see Table S1 and supplementary information). All

models consistently record two peaks in deposition rate, one at around 36–38 Ma and the second at around 30 Ma, with deposition rates significantly higher throughout all of Unit III compared to the under- and overlying units.

Proximal volcaniclastic deposits can be affected by sediment redistribution in consequence of seafloor sediment failure triggered by flank collapses (e.g., Lebas et al., 2011; Watt et al., 2012) but no imbricated, rafted or remnant blocks or chaotic deposits were observed in the seismic profiles at Site U1438 (see Arculus et al., 2015b). The lack of seismically defined chaotic deposits is not surprising in that the site is >50 km away from the arc axis, where such units might be represented by thin slump-generated turbidites or debrites. The sequence drilled at U1438 formed mainly by downslope remobilization of volcaniclastic arc apron deposits, perhaps triggered by over-steepening of slopes on the submarine arc volcanic front, volcanic eruptions, seismic events, or some combination of the above. Furthermore, the 1.6–2.0 Ma periodicity in the volcaniclastic sequence at U1438 reported by Johnson (2016) corresponds well with the lifespan of individual volcanic systems reported from other magmatic arcs including the Taupo Volcanic Zone (>1.6 Ma; Wilson et al., 1995) or the Lesser Antilles (e.g., Silver Hills on Montserrat: 1.4 Ma; Harford et al., 2002). Each episode may thus represent a distinct volcanic system with recurrence intervals of individual sector collapses typically on the order of a few 10s to several 100s ka as a function of tectonic activity and/or magma production rate (Samper et al., 2008). Offshore Montserrat, enhanced rates of volcaniclastic deposition (380–790 m Ma^{-1} proximal and ~530 m Ma^{-1} more distal) are directly linked with volcanic edifice maturity (Watt et al., 2012). Site U1438 is probably more distal than the records from Montserrat but deposition rates are in a similar range (generally 50–150 m Ma^{-1}) and peak at 480 m Ma^{-1} (Table S1; Johnson, 2016). We conclude that Site U1438 represents a unique record of at least four individual volcanic episodes of active island arc magmatism along the nearby KPR.

4.2. The glass inclusion record of Site U1438

Glass inclusions can provide detailed insights into magmatic systems since they represent distinct magma batches trapped during melt ascent from the mantle source region to the surface. In this respect, olivine and spinel are the preferred minerals since they are the first phases to crystallize and as such potentially trap the most primitive melt compositions. However, olivine is prone to alteration through seawater and high-pH porefluids (Oelkers, 1999) and spinel is possibly too dense to be transported over large distances in turbidity currents. As a result, clinopyroxene is the most common mineral phase in the sampled intervals of Site U1438 and hosts a large number of glass inclusions. As described before, we used a number of criteria to ensure that our dataset is not biased through post-entrapment equilibration and boundary crystallization and a thorough discussion is provided in the supplementary information. However, the differences between the distinct groups and the temporal trends of the internally consistent dataset presented here are resistant to modifying processes. Systematic changes in size or shape of the glass inclusion that could result from a non-random occurrence of these alteration processes have not been observed. Furthermore, a number of trace elements (i.e. the medium to heavy REE and Y) have similar partition coefficients between melt and clinopyroxene (e.g., Green et al., 2000) and thus thin reaction boundaries observed at some of the inclusions (Fig. 3) are not sufficient to significantly fractionate these elements between inclusion and host.

The U1438 glass inclusions record a wide range of melt composition from basalt to rhyolite with different evolutionary trends ('calc-alkalic' vs. tholeiitic; Fig. 4). These differing magma trends are clearer when the data are split into two groups according to their deposition age. The older (>37 Ma) group is composed mainly of ('calc-alkalic') high-Mg andesites. The flat shape of the REE patterns closely resembles that of the high-Mg andesites recovered from the Bonin Ridge in the IBM forearc (Fig. 6; Ishizuka et al., 2006). These high-Mg andesites are likely of primary origin (as opposed to products of magma mixing, e.g., at Mt. Shasta; Streck et al., 2007) as indicated for example by their low Sr/Y, mantle-derived origin (glass Mg#s of 65–70 and corresponding cpx host Mg#s of 89–92 are common) and continuous melt evolution. In contrast to these high-Mg andesitic melts, younger inclusions with deposition ages <37 Ma are mainly arc tholeiites and related differentiates. Their REE patterns are generally more enriched, especially in the light to medium REE (La to Sm) and resemble the tholeiitic to 'calc-alkalic' andesite suite from the Bonin Ridge (Fig. 6; Ishizuka et al., 2006).

It is noted that the record of melt compositions with a high-Mg andesite composition (i.e. 'transitional suite') at Site U1438 is significantly younger than reported from other sections of the IBM (Ishizuka et al., 2011a). Interestingly, the evolution from 'calc-alkalic' to tholeiitic rocks observed at Site U1438 contradicts the generally accepted temporal sequence for island arcs developing from tholeiitic through to 'calc-alkalic' rocks and shoshonitic (Jakeš and White, 1972). Furthermore, our data show that 'calc-alkalic' rocks *per se* may not have higher alkali contents than island arc tholeiites (Figs. 4A, D).

4.3. Island arc evolution recorded at Site U1438

According to the model of Ishizuka et al. (2011b), the location of Site U1438 would likely have been influenced simultaneously by arc front and rear arc volcanism in its earliest stages (Eocene), with locally increasing influence of rear arc volcanism younger than 35 Ma and prior to arc rifting at 25 Ma (Oligocene). Nichols et al. (2012) used olivine-hosted glass inclusions to investigate spatial changes across the currently active northern Izu arc: arc front magmas (low-K series) show the strongest influence of a shallow subduction component (i.e., fluid) reflected in high Ba relative to Nb, Th or Yb (see Pearce et al., 2005). In contrast, melts erupted with increasing distance behind the arc front show increasing influence of a deep subduction component (i.e., sediment melt) in that they have high Th relative to Nb or Yb, high Ce/Pb and elevated light REE and are associated with the medium-K series (see Pearce et al., 2005; Skora and Blundy, 2010; Nichols et al., 2012). Imprinted on these 'local' processes, Straub (2003) suggested that the ultrarefractory mantle present following subduction initiation (i.e. the source of boninite volcanism) is gradually replaced by (more fertile) Indian MORB mantle during the Eocene as reflected in highly immobile trace elements that are sensitive to the fertility of the mantle source (e.g., Nb/Yb; Pearce et al., 2005).

In order to identify the relative contributions from these three components, we have compiled representative data for FAB, boninite, arc front and reararc melt compositions from the IBM system in Fig. 6. Among these groups, FAB have the lowest subduction input (i.e., low Ba and Th relative to Yb or Nb; Fig. 7A–D) but the most fertile mantle source (i.e. high Nb relative to Yb, Fig. 7E). At first glance, the >37 Ma group seem to record higher Ba relative to Nb (Fig. 7A) similar to other glass inclusions from the active IBM. The younger (<37 Ma) group, in contrast, records lower Ba relative to Nb similar to andesites from the Bonin Ridge. However, using Th as a tracer for the deep (i.e., sediment) subduction component, all data fall almost on an identical trajectory relative to Nb (Fig. 7B). By comparing Ba and Th to Nb only, we would thus conclude that the group >37 Ma was more influenced by a shallow subduction component relative to the <37 Ma group. However, Pearce et al. (2005) have shown that abundances of Nb in wedge sources are

variable. Indeed, if we compare Ba, Th and Nb to Yb (an element that is independent from a "lithosphere" component; Pearce et al., 2005), the relative contributions of subduction components change significantly. Barium relative to Yb, for example, is similar in both groups, with some inclusions from the older group recording even lower Ba concentrations (at a given Yb) than the <37 Ma group (Fig. 7C). A similar pattern is observed in Th vs. Yb (Fig. 7D), where both groups show a broad overlap with the >37 Ma group extending to lower Th and the <37 Ma to higher Th at a given Yb.

These patterns can be explained by the differences in Nb relative to Yb in the two groups (Fig. 7E). The >37 Ma group tends to have lower Nb at a given Yb than the <37 Ma group (and vice versa) despite a broad overlap. To change these trace elemental systematics significantly, post-entrapment crystallization of cpx would have to exceed 20 Vol.% (see model curves in Fig. 7). We consider this to be unlikely because: 1) cpx boundary crystallization does not significantly affect most trajectories of these elemental pairs; and 2), invocation of differential cpx crystallization is an ad hoc explanation to account for a difference between two groups of an internally consistent dataset (i.e. all U1438 data shown in Fig. 7 are cpx-hosted). To summarize, an increased contribution from a deep subduction component (e.g., Th/Yb) and refertilization (e.g., Nb/Yb) of the mantle wedge is indicated with progressive 'life' of the arc. This view is supported by the range in fluid mobile elements such as Pb or U that is similar in both groups but accompanied by increasing Ce or Th (deep subduction component) with younging (Figs. 8A, B). In fact, overall the light REE that are plausibly controlled by the deep subduction component (Pearce et al., 2005; Skora and Blundy, 2010) are both enriched in the <37 Ma group relative to the medium and heavy REE, and also relative to the older group (Fig. 6). An overall decrease in degree of partial melting through time could explain some of the trace element variation observed. However, a more fundamental geodynamic process is required to explain all of the patterns observed including the major increase in TiO_2 with time (Fig. 4B) and the concomitant progressive change from the 'calk-alkalic' (low-Fe) to the tholeiitic (medium-Fe) association (Fig. 4C). Some inclusions younger than 30 Ma indicate an overall decreasing slab contribution (e.g., lower Ba/La, higher Ce/Pb) that may be attributed to a greater proportion of decompression melting. Such melts share geochemical signatures of both, arc and backarc and may have formed in a pre-rift phase of the arc, possibly along small regions of upwelling mantle that, following arc rifting and backarc extension, commonly link volcanic centers of the arc front and backarc in form of so-called 'hot fingers' (e.g., Tamura et al., 2002).

4.4. Turbocharging the arc

During the time period when the proto-IBM arc was dominated by boninitic melts (evident from the forearc record as 48–44 Ma; e.g., Ishizuka et al., 2011a), arc-derived sediment deposition rates were low (<11 m Ma^{-1}; Table S1) at Site U1438. This may indicate that boninitic magmatism was focused closer to the trench or more restricted across-strike with subdued topography less likely to generate far-traveled gravity flows.

The transition from Unit IV into Unit III at Site U1438 reflects a sharp increase in the rate of deposition (Fig. 2) which we think reflects the onset of the topographically prominent, stratovolcano-building stage of the arc. The precise timing of this transition is yet to be determined but the time frame (40–46 Ma, most likely 44–46 Ma; Fig. 2) is consistent with the transition from boninitic to arc tholeiitic and 'calc-alkalic' lavas across the IBM (i.e., transitional suite of Ishizuka et al., 2011a). However, we have evidence at Site U1438 for a prolonged (or delayed) transitional period with high-Mg andesitic melts dominating over arc tholeiitic melts at least until 37 Ma. The transition from a high-Mg andesitic into

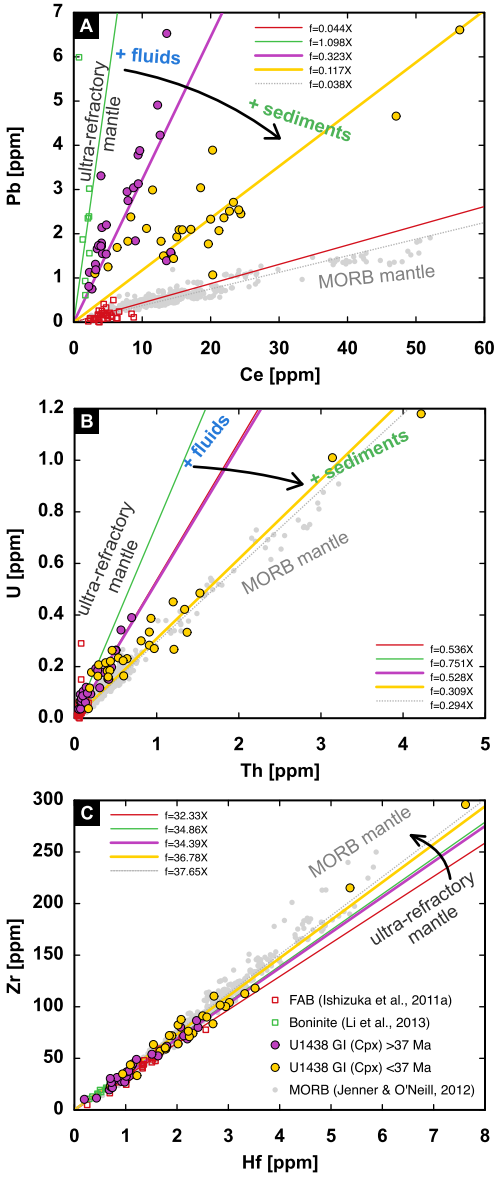

Fig. 8. A) Pb v. Ce, B) U vs. Th and C) Zr vs. Hf (all in ppm). Note the steep slopes of boninites and U1438 GI (Cpx) >37 Ma data in A) and B) that indicate a strong influence of slab fluids (Pb, U). With decreasing age (i.e., U1438 GI (Cpx) <37 Ma group), samples become enriched in Ce and Th attributed to an enhanced contribution from sediments to the KPR arc magmas. High field-strength element systematics (C) indicate a progressive enrichment of Zr relative to Hf over time (mantle wedge replenishment). Regressions have been fitted through the origin. Data as in Fig. 6; MORB: Jenner and O'Neill (2012), filtered for MOR origin.

an arc tholeiitic magma domain is accompanied by at least threefold increase in deposition rate (Fig. 9) that indicates a significant increase in magma production rate. Simultaneously, the deep subduction component (i.e., sediment melt) becomes more pronounced and the increase in Nb relative to Yb or Zr (or Zr/Hf; Fig. 8C) indicates an increasing fertility of the mantle source. The change in Nb/Yb or Nb/Zr cannot result from a bias in the dataset (the <37 Ma group has lower Mg# on average) since no correlation between these ratios and SiO_2 is observed (Fig. S7). We conclude the change in magma source domains resulting in the transition from high-Mg andesitic (i.e. transitional suite) to arc tholeiitic is driven by a refertilization (or replenishment) of the mantle wedge accompanied by an increased contribution from the deep subduction component. We note that deposition rates de-

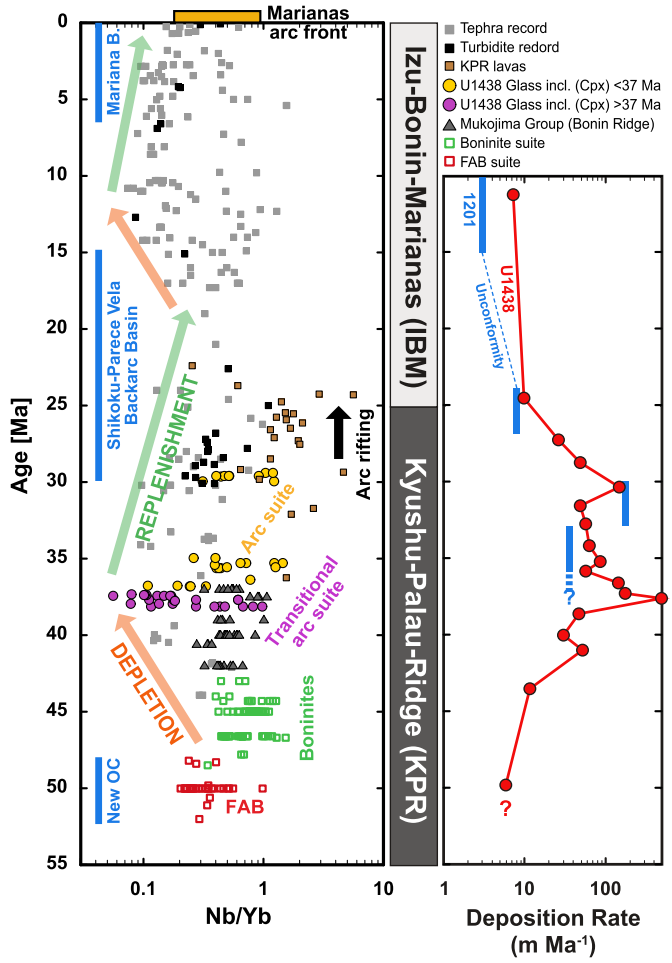

Fig. 9. Age [Ma] plotted vs. Nb/Yb and deposition rate [m Ma^{-1}]. Also shown are major rifting/spreading events in the IBM and our interpretation of the long-term trends observed in Nb/Yb reflecting periods of decreased ("depletion") or enhanced ("replenishment") wedge corner flow. Deposition rates for Site 1201 from Salisbury et al. (2006) and Site U1438 (see also Table S1). Data for IBM Tephra (and clast) record: Arculus and Bloomfield (1992), Bryant et al. (2003), Savov et al. (2006), Straub (2003), Straub et al. (2004, 2015); IBM Turbidite record: Gill et al. (1994); KPR lava: Ishizuka et al. (2011b); Mukojima Group (Bonin Ridge): Kanayama et al. (2014); Boninite Suite: Kanayama et al. (2012), Li et al. (2013); Marianas arc front: Olivine-hosted glass inclusions from the Mariana arc front: Brounce et al. (2014).

crease only slightly after 36 Ma remaining relatively high at an average of ~50 m Ma^{-1} (Fig. 9).

A second peak in deposition rates (~145 m Ma^{-1}) between 31 and 29.5 Ma (Fig. 9) is coincident with initial arc rifting (Ishizuka et al., 2011b). Consistently, glass inclusions <30 Ma reflect a hybrid arc-backarc magma source (i.e., Ba/La and Ce/Pb of about 10; see discussion above). This second peak in deposition rate may reflect an increase in magmatic activity (and also tectonic activity) prior to or during arc rifting and has also been observed in the Tonga-Kermadec subduction system (Clift and ODP Leg 135 Scientific Party, 1994). There, the magmatic maximum is followed by a sharp end to any volcaniclastic sediment supply from the remnant part of the island arc once magmatism focuses along the backarc spreading center. Site U1438 records a similar decrease in depositional rate during the time of medium-K rear-arc volcanism along the KPR (29.3–24.8 Ma; Ishizuka et al., 2011b; ~Unit II; Figs. 2, 9) before magmatic activity and volcaniclastic sediment supply ceased with the onset of backarc spreading in the Shikoku and Parece Vela Basins. As a result, hemipelagic sedimentation dominates the upper part of the sequence (Unit I; Figs. 2, 9).

The volcanic productivity of the arc as expressed by deposition rates of volcaniclastic sediments is thus directly related to the average melt composition and source (i.e. mantle wedge) fertility (Fig. 9).

4.5. Possible causes for mantle wedge replenishment

Subduction may initiate as a consequence of plate reorientation and super-fast slab roll-back but the fundamental causes and mechanisms are still actively debated (Leng and Gurnis, 2015; Arculus et al., 2015a, 2016; Keenan and Encarnación, 2016). Less controversial is the geologic record of subduction initiation that starts with decompression melting of a refractory mantle source accompanied by the minor addition of a subduction component to generate an extensive area of new oceanic crust with a FAB signature (Ishizuka et al., 2011a; Arculus et al., 2015a; Reagan et al., 2010, 2015; Fig. 10). It has to be noted though that in the light of 'FAB' sampled in forearc and reararc settings and some compositional variability, term and definition of 'forearc basalt' need to be reconsidered.

The residual ultra-refractory material in the mantle wedge (~20% melt depletion relative to a fertile MORB mantle; Pearce et al., 1992) then becomes the source for the extraction of boninites due to the addition of large volumes of subduction fluids (e.g., Pearce et al., 1992; Fig. 8), lasting for about 4 Ma (48–44 Ma; e.g., Ishizuka et al., 2011a, 2006; Fig. 10). A similar scenario of a spreading center capturing early subduction zone magmatism and followed by a change in magmatism from tholeiitic to boninitic has been suggested for the Troodos Ophiolite (Regelous et al., 2014). The mantle wedge during arc inception was occupied by material of the Pacific-type MORB domain (Savov et al., 2006; Hickey-Vargas et al., 2006; Straub et al., 2009, 2010, 2015). A ~3 Ma long period of transitional arc magmatism followed (high-Mg andesites; e.g., Ishizuka et al., 2011a, 2006) during which the mantle wedge of the Pacific-type MORB domain became progressively replaced by mantle with an Indian-type MORB signature (Straub, 2003; Straub et al., 2009, 2010, 2015). This Indian-type MORB signature has also been recorded from the Philippine Sea Plate (e.g., Hickey-Vargas, 1998; Hickey-Vargas et al., 2006; Straub et al., 2009) and we think that the refertilization/replenishment observed at Site U1438 is linked to the exchange of these two mantle domains in the mantle wedge. The 'delayed' change we observed (i.e. ~36–38 Ma) may be attributed to a progressive but rather slow exchange of material (i.e. no sharp boundary between the mantle domains), the progression of wedge replenishment along the IBM system from the North to the South (Straub et al., 2015), or diversification of the mantle wedge in response to regional tectonics (Pearce et al., 2005).

Several studies (Straub, 2003; Straub et al., 2015) and also the compositional patterns observed at Site U1438 (Figs. 7, 8) suggest that the primary control of IBM arc magmas is indeed the composition of the mantle wedge (external control) rather than the impact of subducted slab assemblages alone (internal control). Over the lifetime of the IBM system, specific events such as episodic backarc formation (Clark et al., 2008) influence the mantle wedge composition, which in turn controls average melt composition and possibly also the arc front output (Fig. 9).

Oligocene turbidites from the IBM forearc (Gill et al., 1994) add an important perspective to the further understanding of this process. These turbidites record the average composition of melts produced on the eastward migrating part of the KPR that later forms the modern IBM arc. Bulk rock samples from the oldest turbidites after arc rifting (~25 Ma) have the highest Nb/Yb but become more depleted with time (Fig. 9). This pattern is less pronounced but similar to what we observe after subduction initiation (but without the boninite stage; Fig. 9). The effects of backarc

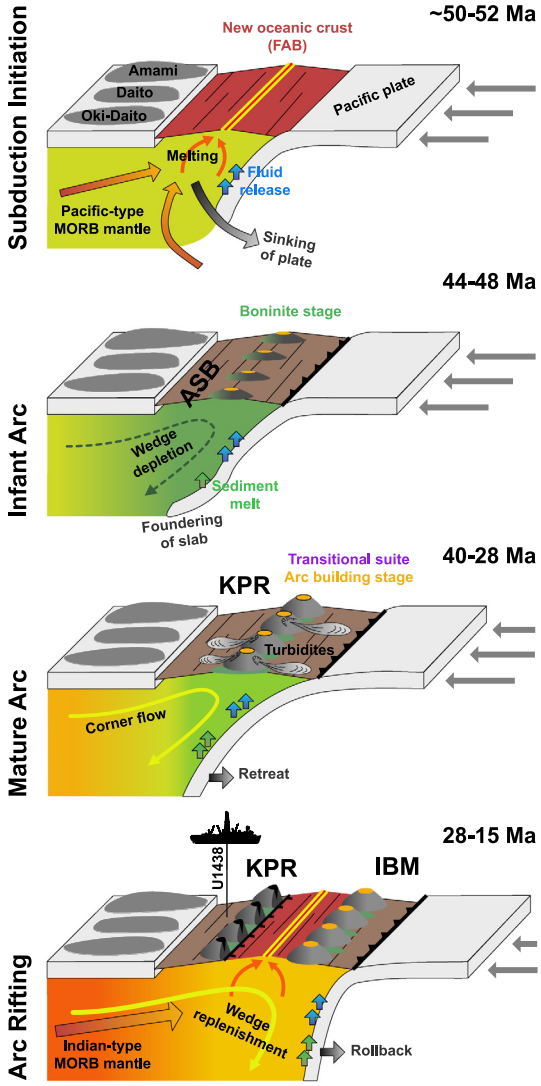

Fig. 10. Sketch of IBM evolution based on earlier models (e.g., Stern and Bloomer, 1992; Ishizuka et al., 2006) and this study. A dynamic slab controls the mantle wedge from subduction initiation about 50–52 Ma ago over the infant arc stage (44–48 Ma) and mature arc stage (28–40 Ma) to cessation of magmatism at the KPR due to rifting and backarc opening (15–28 Ma). During the initial stage, sinking of the slab releases fluids that mixed into the magma in a decompression melting zone of relatively fertile mantle. During the infant arc stage, the local tectonics change from extension to compression, the mantle wedge stagnates and gets progressively more depleted. High fluid flux drives mantle melting to produce boninites. Foundering of the slab and retreat of the trench enhance wedge corner flow with the result of wedge replenishment. The arc building stage begins with the average melt composition changing from boninite to 'calc-alkaline' high-Mg andesite (transitional suite) and finally arc tholeiites with a strong shallow and deep subduction component. Wedge replenishment peaks with trench rollback, arc rifting and backarc opening and results in decompression melting in the Shikoku and Parece Vela Basins and the rise of the modern IBM arc.

spreading (i.e. enhanced corner flow/wedge replenishment) on the subduction system may thus be similar to the process of subduction initiation in terms that large volumes of basaltic melt are extracted from the mantle (backarc basin basalt and FAB, respectively), forming a progressively more refractory mantle that serves as the mantle source for 'calc-alkalic' melts erupted at the arc front.

Thus, the KPR-IBM subduction system is characterized by a "non-steady-state arc geochemical evolution" (Gill et al., 1994) following subduction initiation in the Early Eocene, maturing of the arc and periodic arc rifting (Shikoku-Parece Vela Basin, Mariana Trough; Fig. 10). This emphasizes the importance of changes in the melt source region linking to replenishment of the mantle wedge by material extracted from the subducting slab and influx of more fertile mantle material (i.e., the Indian-type MORB mantle). Where mantle wedge rejuvenation is incomplete or parts of the wedge are being 'trapped' in the mantle wedge corner (stagnation), boninites could erupt independently of a juvenile arc phase (e.g., Tonga; Cooper et al., 2010).

4.6. A dynamic control?

Infant arc spreading (i.e. formation of new oceanic crust with a FAB signature) requires an extensional tectonic regime in an overall convergent environment (Leng et al., 2012). Foundering of the slab and trench retreat favor asthenospheric upwelling, decompression melting and formation of new oceanic crust with a geochemical FAB signature (Fig. 10). In subduction systems where ridge push drives constant stress (no trench migration) boninites can still be produced but new oceanic crust is not being formed (Leng et al., 2012). Thus, the sequence of boninite following FAB is consistent with both contrasting modes of subduction initiation (i.e., induced vs. spontaneous) but not with a constant stress regime. However, recent results from IODP Exp. 351 favor (Arculus et al., 2015a, 2016) or are at least consistent with the model of spontaneous subduction initiation (Leng and Gurnis, 2015). Furthermore, the missing far field stress field consistent with spontaneous subduction initiation may promote infant arc spreading.

During arc infancy, the preferential downdip sinking of the slab may induce an only "sluggish" flow in the mantle wedge (Kincaid and Griffiths, 2003) that would then enhance the residence time of the refractory mantle source residual to FAB extraction and the source for subsequent boninite melt extraction (Fig. 10). This scenario would be consistent with further depletion of the mantle source (FAB to high-Ca boninites to low-Ca boninites) as observed in the IBM forearc by Pearce et al. (1992). Foundering of the slab finally results in trench retreat (Leng and Gurnis, 2011; 15 mm a^{-1} in the IBM system: Stern and Bloomer, 1992) and induces a strong mantle flow (Kincaid and Griffiths, 2003). The induced flow in the mantle wedge may control the progressive replenishment of the mantle wedge that leads to the transition in the average magmatic output of the arc from boninites to 'calc-alkalic' high-Mg andesites to arc tholeiites observed at Site U1438 (this study) and elsewhere in the IBM (e.g., Ishizuka et al., 2011a and references therein; Fig. 10). Increased temperatures as a consequence of higher velocities of the mantle flow (Kincaid and Griffiths, 2003) likely also promote the influence of a deep subduction component (i.e., sediment melts). The evolution of magmatism in the IBM from FAB over boninites to 'normal' arc magmatism is almost synchronous (Ishizuka et al., 2011a) and thus consistent with a slab-dynamic control.

We suggest the boninite and 'calc-alkalic' high-Mg andesite stages of arc evolution may endure as long as mantle wedge sources are not advected away from zones of arc magma generation, or the rate of wedge replenishment by corner flow does not overwhelm the rate of magma extraction.

5. Conclusions

IODP Expedition 351 Izu–Bonin–Mariana Arc Origins recovered a unique section of volcaniclastic sediments that records the full lifespan of the Kyushu–Palau Ridge, the proto-IBM island arc. These sediments were transported from the volcanic source to the drill location by gravity flows in response to numerous eruption events. The sediments reflect the continuous magmatic output of the island arc system and glass inclusions preserved in unaltered minerals provide insights into the evolution of the island arc in

terms of average melt composition and relative timing. Our conclusions based on the combined study of volcaniclastic sediments and mineral-hosted glass inclusions are:

- In the case of the IBM system, the sequence of rock types is not boninitic-tholeiitic-'calc-alkalic'-shoshonitic as suggested for example by Jakeš and White (1972). Instead, island arc magmatism commences with the 'calc-alkalic' rock series (boninites and high-Mg andesites) and then evolves into a system dominated by arc tholeiites.
- The change from the 'calc-alkalic' juvenile stage to the arc tholeiitic mature stage of the island arc is coincident with a substantial increase in the volcanic output of the arc. Later, deposition rates peak again just before rifting of the arc.
- Arc magma compositions following subduction initiation are dynamically controlled by mantle source fertility as a function of wedge corner flow.

Acknowledgements

This study used samples provided by the IODP. The authors thank the JR crew and IODP staff of Exp. 351, in particular our great staff scientist K. Bogus. We highly appreciate the great effort of all expedition participants. We like to thank editor Tamsin Mather and two anonymous reviewers for their constructive comments and helpful suggestions. PAB thanks IODP Germany for supporting his participation on Expedition 351, ANZIC for funding of the analytical work through a grant to RJA, and the Alexander von Humboldt Foundation for his Feodor Lynen Research Fellowship. Contributions by KMM and KJ were supported by grants from the National Science Foundation (OCE-1503694) and from the Consortium for Ocean Leadership US Science Support Program. IPS thanks UK IODP (NE/M007782/1) for funding.

Appendix A. Supplementary material

Supplementary material related to this article can be found online at http://dx.doi.org/10.1016/j.epsl.2016.12.027.

References

Allen, S.R., Hayward, B.W., Mathews, E., 2007. A facies model for a submarine volcaniclastic apron: the Miocene Manukau Subgroup, New Zealand. Geol. Soc. Am. Bull. 119, 725–742. http://dx.doi.org/10.1130/B26066.1.

Arculus, R.J., 2003. Use and abuse of the terms calcalkaline and calcalkalic. J. Petrol. 44, 929–935. http://dx.doi.org/10.1093/petrology/44.5.929.

Arculus, R.J., Bloomfield, A.L., 1992. Major element geochemistry of ashes from Sites 782, 784 and 786 in the Bonin forearc. In: Fryer, P., et al. (Eds.), Proceedings of the Ocean Drilling Program, Scientific Results, vol. 125. Ocean Drilling Program, College Station, TX, pp. 277–292.

Arculus, R.J., Ishizuka, O., Bogus, K.A., Gurnis, M., Hickey-Vargas, R., Aljahdali, M.H., Bandini-Maeder, A.N., Barth, A.P., Brandl, P.A., Drab, L., do Monte Guerra, R., Hamada, M., Jiang, F., Kanayama, K., Kender, S., Kusano, Y., Li, H., Loudin, L.C., Maffione, M., Marsaglia, K.M., McCarthy, A., Meffre, S., Morris, A., Neuhaus, M., Savov, I.P., Sena, C., Tepley III, F.J., van der Land, C., Yogodzinski, G.M., Zhang, Z., 2015a. A record of spontaneous subduction initiation in the Izu–Bonin–Mariana arc. Nat. Geosci. 8, 728–733. http://dx.doi.org/10.1038/ngeo2515.

Arculus, R.J., Ishizuka, O., Bogus, K.A., Aljahdali, M.H., Bandini-Maeder, A.N., Barth, A.P., Brandl, P.A., do Monte Guerra, R., Drab, L., Gurnis, M., Hamada, M., Hickey-Vargas, R., Jiang, F., Kanayama, K., Kender, S., Kusano, Y., Li, H., Loudin, L.C., Maffione, M., Marsaglia, K.M., McCarthy, A., Meffre, S., Morris, A., Neuhaus, M., Savov, I.P., Sena, C., Tepley III, F.J., van der Land, C., Yogodzinski, G.M., Zhang, Z., 2015b. Site U1438. In: Arculus, R.J., Ishizuka, O., Bogus, K.A., Expedition 351 Scientists (Eds.), Expedition Izu–Bonin–Mariana Arc Origins. In: Proceedings of the International Ocean Discovery Program. International Ocean Discovery Program, College Station, TX.

Arculus, R.J., Ishizuka, O., Bogus, K.A., Gurnis, M., Hickey-Vargas, R., Aljahdali, M.H., Bandini-Maeder, A.N., Barth, A.P., Brandl, P.A., Drab, L., do Monte Guerra, R., Hamada, M., Jiang, F., Kanayama, K., Kender, S., Kusano, Y., Li, H., Loudin, L.C., Maffione, M., Marsaglia, K.M., McCarthy, A., Meffre, S., Morris, A., Neuhaus, M., Savov, I.P., Sena, C., Tepley III, F.J., van der Land, C., Yogodzinski, G.M., Zhang, Z., 2016. Reply to 'Unclear causes of subduction'. Nat. Geosci. 9, 338–339. http://dx.doi.org/10.1038/ngeo2704.

Brounce, M.N., Kelley, K.A., Cottrell, E., 2014. Variations in $Fe^{3+}/\sum Fe$ of Mariana arc basalts and mantle wedge fO_2. J. Petrol. 55, 2513–2536. http://dx.doi.org/10.1093/petrology/egu065.

Bryant, C.J., Arculus, R.J., Eggins, S.M., 2003. The geochemical evolution of the Izu–Bonin arc system: a perspective from tephras recovered by deep-sea drilling. Geochem. Geophys. Geosyst. 4, 1094. http://dx.doi.org/10.1029/2002GC000427.

Clark, S.R., Stegman, D., Müller, R.D., 2008. Episodicity in back-arc tectonic regimes. Phys. Earth Planet. Inter. 171, 265–279. http://dx.doi.org/10.1016/j.pepi.2008.04.012.

Clift, P.D., ODP Leg 135 Scientific Party, 1994. Volcanism and sedimentation in a rifting island-arc terrain: an example from Tonga, SW Pacific. Geol. Soc. (Lond.) Spec. Publ. 81, 29–51. http://dx.doi.org/10.1144/GSL.SP.1994.081.01.03.

Cooper, L.B., Plank, T., Arculus, R.J., Hauri, E.H., Hall, P.S., Parman, S.W., 2010. High-Ca boninites from the active Tonga Arc. J. Geophys. Res. 115, B10206. http://dx.doi.org/10.1029/2009jb006367.

Davidson, J.P., Arculus, R.J., 2005. The significance of Phanerozoic arc magmatism in generating continental crust. In: Evolution and Differentiation of the Continental Crust, pp. 136–173.

Gill, J.B., Hiscott, R.N., Vidal, P., 1994. Turbidite geochemistry and evolution of the Izu–Bonin arc and continents. Lithos 33, 135–168. http://dx.doi.org/10.1016/0024-4937(94)90058-2.

Green, T.H., Blundy, J.D., Adam, J., Yaxley, G.M., 2000. SIMS determination of trace element partition coefficients between garnet, clinopyroxene and hydrous basaltic liquids at 2–7.5 GPa and 1080–1200 C. Lithos 53, 165–187.

Harford, C.L., Pringle, M.S., Sparks, R.S.J., Young, S.R., 2002. The volcanic evolution of Montserrat using $^{40}Ar/^{39}Ar$ geochronology. Mem. Geol. Soc. Lond. 21, 93–113.

Hickey-Vargas, R., 1998. Origin of the Indian Ocean-type isotopic signature in basalts from Philippine Sea plate spreading centers: an assessment of local versus large-scale processes. J. Geophys. Res., Solid Earth 103, 20963–20979. http://dx.doi.org/10.1029/98jb02052.

Hickey-Vargas, R., Savov, I.P., Bizimis, M., Ishii, T., Fujioka, K., 2006. Origin of diverse geochemical signatures in igneous rocks from the West Philippine Basin: implications for tectonic models. Geophys. Monogr. Ser. 166, 287–303. http://dx.doi.org/10.1029/166gm15.

Houghton, B.F., Landis, C.A., 1989. Sedimentation and volcanism in a Permian arc-related basin, southern New Zealand. Bull. Volcanol. 51, 433–450. http://dx.doi.org/10.1007/BF01078810.

Ishizuka, O., Kimura, J., Li, Y., Stern, R., Reagan, M., Taylor, R., Ohara, Y., Bloomer, S., Ishii, T., Hargrove III, U., 2006. Early stages in the evolution of Izu–Bonin arc volcanism: new age, chemical, and isotopic constraints. Earth Planet. Sci. Lett. 250, 385–401. http://dx.doi.org/10.1016/j.epsl.2006.08.007.

Ishizuka, O., Tani, K., Reagan, M.K., Kanayama, K., Umino, S., Harigane, Y., Sakamoto, I., Miyajima, Y., Yuasa, M., Dunkley, D.J., 2011a. The timescales of subduction initiation and subsequent evolution of an oceanic island arc. Earth Planet. Sci. Lett. 306, 229–240. http://dx.doi.org/10.1016/j.epsl.2011.04.006.

Ishizuka, O., Taylor, R.N., Yuasa, M., Ohara, Y., 2011b. Making and breaking an island arc: a new perspective from the Oligocene Kyushu–Palau arc, Philippine Sea. Geochem. Geophys. Geosyst. 12, Q05005. http://dx.doi.org/10.1029/2010GC003440.

Jakeš, P., White, A.J.R., 1972. Major and trace element abundances in volcanic rocks of orogenic areas. Geol. Soc. Am. Bull. 83, 29–40.

Jenner, F.E., O'Neill, H.S.C., 2012. Analysis of 60 elements in 616 ocean floor basaltic glasses. Geochem. Geophys. Geosyst. 13, Q02005. http://dx.doi.org/10.1029/2011GC004009.

Jochum, K.P., Dingwell, D.B., Rocholl, A., Stoll, B., Hofmann, A.W., Becker, A., Besmehn, A., Bessette, D., Dietze, H.-J., Dulski, P., Erzinger, J., Hellebrand, E., Hoppe, P., Horn, I., Janssens, K., Jenner, G.A., Klein, M., McDonough, W.F., Maetz, M., Mezger, K., Münker, C., Nikogosian, I.K., Pickhardt, C., Raczek, I., Rhede, D., Seufert, H.M., Simakin, S.G., Sobolev, A.V., Spettel, B., Straub, S., Vincze, L., Wallianos, A., Weckwerth, G., Weyer, S., Wolf, D., Zimmer, M., 2000. The preparation and preliminary characterisation of eight geological MPI-DING reference glasses for in-situ microanalysis. Geostand. Newsl. 24, 87–133.

Johnson, K., 2016. Facies and Depositional History of Arc-Related, Deep-Marine Volcaniclastic Rocks in Core Recovered on International Ocean Discovery Program Expedition 351, Philippine Sea. MSc thesis. California State University Northridge. doi:10211.3/172640.

Kanayama, K., Umino, S., Ishizuka, O., 2012. Eocene volcanism during the incipient stage of Izu-Ogasawara Arc: geology and petrology of the Mukojima Island Group, the Ogasawara Islands. Isl. Arc 21, 288–316. http://dx.doi.org/10.1111/iar.12000.

Kanayama, K., Umino, S., Ishizuka, O., 2014. Shallow submarine volcano group in the early stage of island arc development: geology and petrology of small islands south off Hahajima main island, the Ogasawara Islands. J. Asian Earth Sci. 85, 1–25. http://dx.doi.org/10.1016/j.jseaes.2014.01.012.

Keenan, T.E., Encarnación, J., 2016. Unclear causes for subduction. Nat. Geosci. 9, 338. http://dx.doi.org/10.1038/ngeo2703.

Kincaid, C., Griffiths, R.W., 2003. Laboratory models of the thermal evolution of the mantle during rollback subduction. Nature 425, 58–62. http://dx.doi.org/10.1038/nature01923.

Le Bas, M.J., 2000. IUGS reclassification of the high-Mg and picritic volcanic rocks. J. Petrol. 41, 1467–1470. http://dx.doi.org/10.1093/petrology/41.10.1467.

Le Bas, M.J., Le Maitre, R.W., Streckeisen, A., Zanettin, B., 1986. A chemical classification of volcanic rocks based on the total alkali-silica diagram. J. Petrol. 27, 745–750. http://dx.doi.org/10.1093/petrology/27.3.745.

Lebas, E., Le Friant, A., Boudon, G., Watt, S.F.L., Talling, P.J., Feuillet, N., Deplus, C., Berndt, C., Vardy, M.E., 2011. Multiple widespread landslides during the long-term evolution of a volcanic island: insights from high-resolution seismic data, Montserrat, Lesser Antilles. Geochem. Geophys. Geosyst. 12, Q05006. http://dx.doi.org/10.1029/2010GC003451.

Le Maitre, R.W., Streckeisen, A., Zanettin, B., Le Bas, M.J., Bonin, B., Bateman, P., Bellieni, G., Dudek, A., Efremova, S., Keller, J., Lameyre, J., Sabine, P.A., Schmid, R., Sorensen, H., Woolley, A.R., 1998. Igneous Rocks – A Classification and Glossary of Terms, 2nd ed. Cambridge University Press, Cambridge.

Leng, W., Gurnis, M., 2011. Dynamics of subduction initiation with different evolutionary pathways. Geochem. Geophys. Geosyst. 12, Q12018. http://dx.doi.org/10.1029/2011GC003877.

Leng, W., Gurnis, M., 2015. Subduction initiation at relic arcs. Geophys. Res. Lett. 42, 7014–7021.

Leng, W., Gurnis, M., Asimow, P., 2012. From basalts to boninites: the geodynamics of volcanic expression during induced subduction initiation. Lithosphere 4, 511–523.

Li, Y.-B., Kimura, J.-I., Machida, S., Ishii, T., Ishiwatari, A., Maruyama, S., Qiu, H.-N., Ishikawa, T., Kato, Y., Takahata, N., Hirahara, Y., Miyazaki, T., 2013. High-Mg adakite and low-Ca boninite from a Bonin fore-arc seamount: implications for the reaction between slab melts and depleted mantle. J. Petrol. 54, egt008–1175. http://dx.doi.org/10.1093/petrology/egt008.

McDonough, W.F., Sun, S., 1995. The composition of the Earth. Chem. Geol. 120, 223–253.

Miyashiro, A., 1974. Volcanic rock series in island arcs and active continental margins. Am. J. Sci. 274, 321–355. http://dx.doi.org/10.2475/ajs.274.4.321.

Nichols, A.R.L., Wysoczanski, R.J., Tani, K., Tamura, Y., Baker, J.A., Tatsumi, Y., 2012. Melt inclusions reveal geochemical cross-arc variations and diversity within magma chambers feeding the Higashi–Izu Monogenetic Volcano Field, Izu Peninsula, Japan. Geochem. Geophys. Geosyst. 13, Q09012. http://dx.doi.org/10.1029/2012GC004222.

Oelkers, E.H., 1999. A comparison of forsterite and enstatite dissolution rates and mechanisms. In: Growth, Dissolution and Pattern Formation in Geosystems. Springer, Dordrecht, pp. 253–267.

O'Neill, H.S.C., 2016. The smoothness and shapes of chondrite-normalized rare Earth element patterns in basalts. J. Petrol. 57, 1463–1508. http://dx.doi.org/10.1093/petrology/egw047.

Pearce, J.A., Stern, R.J., Bloomer, S.H., Fryer, P., 2005. Geochemical mapping of the Mariana arc-basin system: implications for the nature and distribution of subduction components. Geochem. Geophys. Geosyst. 6, Q07006.

Pearce, J.A., Van der Laan, S.R., Arculus, R.J., Murton, B.J., Ishii, T., Peate, D.W., Parkinson, I.J., 1992. Boninite and harzburgite from Leg 125 (Bonin–Mariana forearc): a case study of magma genesis during the initial stages of subduction. In: Proceedings of the Ocean Drilling Program, vol. 125, pp. 623–659.

Putirka, K.D., 2008. Thermometers and barometers for volcanic systems. In: Putirka, K.D., Tepley, F. (Eds.), Reviews in Mineralogy and Geochemistry, pp. 61–120. http://dx.doi.org/10.2138/rmg.2008.69.3.

Reagan, M.K., Hanan, B.B., Heizler, M.T., Hartman, B.S., Hickey-Vargas, R., 2008. Petrogenesis of volcanic rocks from Saipan and Rota, Mariana Islands, and implications for the evolution of nascent island arcs. J. Petrol. 49, 441–464. http://dx.doi.org/10.1093/petrology/egm087.

Reagan, M.K., Ishizuka, O., Stern, R.J., Kelley, K.A., Ohara, Y., Blichert-Toft, J., Bloomer, S.H., Cash, J., Fryer, P., Hanan, B.B., Hickey-Vargas, R., Ishii, T., Kimura, J.-I., Peate, D.W., Rowe, M.C., Woods, M., 2010. Fore-arc basalts and subduction initiation in the Izu–Bonin–Mariana system. Geochem. Geophys. Geosyst. 11, Q03X12.

Reagan, M.K., Pearce, J.A., Petronotis, K., Almeev, R., Avery, A.A., Carvallo, C., Chapman, T., Christeson, G.L., Ferré, E.C., Godard, M., Heaton, D.E., Kirchenbaur, M., Kurz, W., Kutterolf, S., Li, H.Y., Michibayashi, K., Morgan, S., Nelson, W.R., Prytulak, J., Python, M., Robertson, A.H.F., Ryan, J.G., Sager, W.W., Sakuyama, T., Shervais, J.W., Shimizu, K., Whattam, S.A., 2015. Expedition 352 summary. In: Proceedings of the International Ocean Discovery Program, vol. 352, pp. 1–32.

Regelous, M., Haase, K.M., Freund, S., Keith, M., Weinzierl, C.G., Beier, C., Brandl, P.A., Endres, T., Schmidt, H., 2014. Formation of the Troodos Ophiolite at a triple junction: evidence from trace elements in volcanic glass. Chem. Geol. 386, 66–79.

Salisbury, M.H., Shinohara, M., Suetsugu, D., Arisaka, M., Diekmann, B., Januszczak, N., Savov, I.P., 2006. Leg 195 synthesis: Site 1201 – a geological and geophysical section in the West Philippine Basin from the 660 km discontinuity to the mudline. In: Shonohara, M., Salisbury, M.H., Richter, C. (Eds.), Proceedings of the Ocean Drilling Program, Scientific Results, vol. 195. Ocean Drilling Program, College Station, TX, pp. 1–27.

Samper, A., Quidelleur, X., Boudon, G., Le Friant, A., Komorowski, J.C., 2008. Radiometric dating of three large volume flank collapses in the Lesser Antilles Arc. J. Volcanol. Geotherm. Res. 176, 485–492.

Savov, I.P., Hickey-Vargas, R., D'Antonio, M., Ryan, J.G., Spadea, P., 2006. Petrology and geochemistry of West Philippine basin basalts and early Palau–Kyushu arc volcanic clasts from ODP Leg 195, Site 1201D: implications for the early history of the Izu–Bonin–Mariana arc. J. Petrol. 47, 277–299. http://dx.doi.org/10.1093/petrology/egi075.

Shervais, J.W., 1982. Ti–V plots and the petrogenesis of modern and ophiolitic lavas. Earth Planet. Sci. Lett. 59, 101–118. http://dx.doi.org/10.1016/0012-821x(82)90120-0.

Skora, S., Blundy, J., 2010. High-pressure hydrous phase relations of radiolarian clay and implications for the involvement of subducted sediment in arc magmatism. J. Petrol. 51, 2211–2243.

Stern, R.J., Bloomer, S.H., 1992. Subduction zone infancy: examples from the Eocene Izu–Bonin–Mariana and Jurassic California arcs. Geol. Soc. Am. Bull. 104, 1621–1636.

Straub, S.M., 2003. The evolution of the Izu Bonin–Mariana volcanic arcs (NW Pacific) in terms of major element chemistry. Geochem. Geophys. Geosyst. 4, 1018. http://dx.doi.org/10.1029/2002GC000357.

Straub, S.M., Layne, G.D., Schmidt, A., Langmuir, C.H., 2004. Volcanic glasses at the Izu arc volcanic front: new perspectives on fluid and sediment melt recycling in subduction zones. Geochem. Geophys. Geosyst. 5, Q01007. http://dx.doi.org/10.1029/2002GC000408.

Straub, S.M., Goldstein, S.L., Class, C., Schmidt, A., 2009. Mid-ocean-ridge basalt of Indian type in the northwest Pacific Ocean basin. Nat. Geosci. 2, 286–289. http://dx.doi.org/10.1038/ngeo471.

Straub, S.M., Goldstein, S.L., Class, C., Schmidt, A., Gómez-Tuena, A., 2010. Slab and mantle controls on the Sr–Nd–Pb–Hf isotope evolution of the post 42 Ma Izu–Bonin volcanic arc. J. Petrol. 51, 993–1026. http://dx.doi.org/10.1093/petrology/egq009.

Straub, S.M., Woodhead, J.D., Arculus, R.J., 2015. Temporal evolution of the Mariana arc: mantle wedge and subducted slab controls revealed with a tephra perspective. J. Petrol. 56, 409–439. http://dx.doi.org/10.1093/petrology/egv005.

Streck, M.J., Leeman, W.P., Chesley, J., 2007. High-magnesian andesite from Mount Shasta: a product of magma mixing and contamination, not a primitive mantle melt. Geology 35, 351.

Tamura, Y., Tatsumi, Y., Zhao, D., Kido, Y., Shukuno, H., 2002. Hot fingers in the mantle wedge: new insights into magma genesis in subduction zones. Earth Planet. Sci. Lett. 197, 105–116. http://dx.doi.org/10.1016/S0012-821X(02)00465-X.

Watt, S.F.L., Talling, P.J., Vardy, M.E., Masson, D.G., Henstock, T.J., Hühnerbach, V., Minshull, T.A., Urlaub, M., Lebas, E., Le Friant, A., Berndt, C., Crutchley, G.J., Karstens, J., 2012. Widespread and progressive seafloor-sediment failure following volcanic debris avalanche emplacement: landslide dynamics and timing offshore Montserrat, Lesser Antilles. Mar. Geol. 323–325, 69–94.

Wilson, C.J.N., Houghton, B.F., McWilliams, M.O., Lanphere, M.A., Weaver, S.D., Briggs, R.M., 1995. Volcanic and structural evolution of Taupo Volcanic Zone, New Zealand: a review. J. Volcanol. Geotherm. Res. 68, 1–28.